ChemPubSoc Europe
DOI: 10.1002/cphc.201402887
CHEMPHYSCHEM Articles

# Energy Landscape Exploration of Sub-Nanometre Copper–Silver Clusters

Christopher J. Heard,*[a] Roy L. Johnston,[b] and J. Christian Schön[c]

The energy landscapes of sub-nanometre bimetallic coinage metal clusters are explored with the Threshold Algorithm coupled with the Birmingham Cluster Genetic Algorithm. Global and energetically low-lying minima along with their permutational isomers are located for the $Cu_4Ag_4$ cluster with the Gupta potential and density functional theory (DFT). Statistical tools are employed to map the connectivity of the energy landscape and the growth of structural basins, while the thermodynamics of interconversion are probed, based on probability flows between minima. Asymmetric statistical weights are found for pathways across dividing states between stable geometries, while basin volumes are observed to grow independently of the depth of the minimum. The DFT landscape is found to exhibit significantly more frustration than that of the Gupta potential, including several open, pseudo-planar geometries which are energetically competitive with the global minimum. The differences in local minima and their transition barriers between the two levels of theory indicate the importance of explicit electronic structure for even simple, closed shell clusters.

## 1. Introduction

Detailed structural investigation of ultrasmall, gas-phase coinage metal clusters has received a significant amount of experimental[1–5] and theoretical[1,6–14] attention in recent years, particularly since the advent of size-specific cluster generation methods.[1,15] The clusters' potential as electro- and photocatalysts[10,16,17] in addition to their unique optoelectronic properties[18–20] has driven interest in predicting and controlling cluster geometries at the atomic level. Gas-phase clusters represent the fundamental, unperturbed ideal, in the absence of perturbations such as solvent, substrates or bound ligands. For coinage metals, the unambiguous prediction of the geometric structure is complicated by the presence of a high-lying full d electronic band, which plays a significant role in the electronic structure, promoting low coordination and planar structures, which vary with size and charge state. This effect has been found to be adequately described by density functional methods.[6] Empirical and semi-empirical potentials with simple, closed functional forms are commonly used to study the structures of larger clusters, where the parameterisation usually does not account for complex many-body, multi-electron terms, such as correlation or relativistic effects. However, in spite of their lack of complexity, such potentials are often found to be sufficient for neutral, closed-shell systems, and therefore these functions (e.g. Gupta,[21] Sutton–Chen,[22] Murrell–Mottram[23] etc.) are frequently utilised for screening low-lying structures of simple metals, such as alkali metal or group 11 clusters.[9,24–26] The important condition that must be satisfied for this approximation to be valid is that there should be a good correlation between low-lying structures at the empirical potential level and at higher levels, such as DFT. In the absence of such a correlation, more refined parameterisations and/or more complex functional forms are required.

The extension of the analysis beyond static structures is available through the exploration of the underlying potential energy surface, or energy landscape.[27,28] The rearrangement pathways between minima, transition state barriers,[28–30] dynamics[31–33] and basin topology[31,34,35] may be determined by such exploration. At the level of the empirical potential, much research has been done, both in developing efficient methods to explore and map the landscape,[27,36] and to use these tools to elucidate patterns in cluster growth, doping and element type.

In this article, we compare the low-energy structures of a copper–silver sub-nanometre cluster in the gas phase for Gupta potential and DFT levels of theory, and map the energy landscape with a range of statistical tools. This work utilises the threshold algorithm,[31] which has previously been successfully applied to ionic solids,[37–39] molecular clusters[40] and noble metal clusters[41] and has recently been extended to work in tandem with a plane-wave DFT code for direct electronic structure energy landscape exploration. The activation energy barrier heights[30] are calculated for the low-energy region of the Gupta potential energy surface in Section 2.1.1 and the corresponding tree graph of connectivity is generated. Dynamic features are estimated, and the evolution of general-

[a] Dr. C. J. Heard
Department of Applied Physics
Chalmers University of Technology
Gothenburg (Sweden)
E-mail: christopher.heard@chalmers.se
[b] Prof. R. L. Johnston
School of Chemistry
University of Birmingham
Edgbaston, Birmingham (UK)
[c] Prof. Dr. J. C. Schön
Max Planck Institute for Solid-State Research
Heisenbergstrasse 1, 70569 Stuttgart (Germany)

ised energetic-entropic barriers between basins are represented in Section 2.1.2 by the probability flow.[40] In Section 2.1.3, the growth of the densities of configurational states are estimated. Comparison with the structures and barrier heights from DFT calculations are given in Section 2.2.

## Computational Methods

We take a hierarchical approach to exploring the energy landscape of small clusters, based on an unbiased global optimisation of structure, followed by searching the potential energy surface with the threshold method. Sampling of configuration space is performed on-the-fly, in order to collect statistical information regarding the configurational densities of states.

### Models

Part of this investigation is undertaken using a semi-empirical potential function to represent the interactions between metal atoms. The ability of these potentials to reproduce the bonding and preferred structures of clusters is well-tested for large clusters. For sub-nanometre size particles, where the possible structures strongly vary as function of cluster size, and complex quantum effects play an important role in the structure formation, the simplicity of the Gupta potential function does not guarantee a good correlation with higher-level methods. In the current work, we consider copper–silver clusters, which are known to exhibit limited s/d mixing, and a small degree of charge transfer compared to gold-containing clusters, and thus should be fairly well treated by the Gupta potential.[8,21] This potential is derived from the second moment approximation to tight-binding theory, which aims to model the hopping of electrons between atomic sites. The form of the potential, given by Equations (1)–(4), show an attractive many-body term related to the shared electronic density across multiple metal atoms $U_i^{att}$, and a repulsive pair term $U_i^{rep}$, which are summed over all sites to give the total energy $U_{tot}$. The potential contains five parameters $A, q, p, \zeta$ and $r_0$, which are parameterised to empirical values for the cohesive energy, elastic constants, bulk modulus and lattice spacing. The parameters $q, p$ and $r_0$ for mixed bonds are derived from the arithmetic means of the homometallic values. All parameters are as used in recent work,[42] which were originally generated in Ref. [43] [Eq. (1)]:

$$U_{tot} = \sum_i \left[U_i^{rep} + U_i^{att}\right] \quad (1)$$

which is equivalent to Equation (2):

$$U_{tot} = \sum_{i\neq j}\left[\sum_j \theta(r_{ij}) - \left[\xi^2 \sum_j \phi(r_{ij})\right]^{\frac{1}{2}}\right] \quad (2)$$

where [Eq. (3)]:

$$\theta(r_{ij}) = Ae^{-p\left[\left(r_{ij}-r_0\right)/r_0\right]} \quad (3)$$

and [Eq. (4)]:

$$\phi(r_{ij}) = e^{-2q\left[\left(r_{ij}-r_0\right)/r_0\right]} \quad (4)$$

The values used in this study are given in Table 1.

**Table 1.** Parameters for the Gupta potential.

| Element | $A$ | $q$ | $p$ | $\zeta$ | $r_0$ |
|---|---|---|---|---|---|
| Cu–Cu | 0.0894 | 2.430 | 10.55 | 1.2799 | 2.5560 |
| Cu–Ag | 0.0980 | 2.805 | 10.70 | 1.2274 | 2.72405 |
| Ag–Ag | 0.1031 | 3.180 | 10.85 | 1.1895 | 2.89210 |

The result obtained with this parameterisation, which had been designed for a bulk-like metallic system, is likely to differ from the ab initio level result in the small-size regimes we are concerned with in this study, and will be investigated in the following sections. For electronic structure calculations, plane-wave DFT is employed within the Quantum Espresso package,[44] with ultrasoft Rappe–Rabe–Kaxiras–Joannopoulos (RRKJ) pseudopotentials,[45] which contain eleven valence electrons per atom, and the Perdew–Berke–Ernzerhof (PBE)[46] exchange–correlation functional. During threshold algorithm simulations, the convergence criteria are relatively tight, in order to ensure accurate local minimum structures. During local minimisation, the total energy and forces are considered converged when they vary between cycles by less than $10^{-3}$ Ry and $10^{-4}$ Ry/$a_0$, respectively. The Methfessel–Paxton[47] smearing scheme is employed to improve the treatment of metallic states, with a smearing width of 0.005 Ry.

### Structure Prediction

An unbiased global optimisation of clusters in the gas phase is performed at both Gupta and DFT levels of theory, using the Birmingham Cluster Genetic Algorithm (BCGA).[48,49] At the Gupta level of theory, standard GA parameters are employed, as described in Ref. [48]. 100 random seeds are used to create initial geometries, with each generation containing 40 individual clusters. Mating is achieved through a weighted Deaven–Ho crossover method, and mutation is performed by replacement of the selected cluster with a randomly generated new cluster structure, with a probability of 0.1. For the DFT global optimisation, we reduced the population size to ten clusters to improve computational efficiency. The parent selection type (roulette), mating type (weighted, two-point crossover) and generation convergence criteria (five consecutive unchanged minimum energy clusters) were set to be identical between the two levels.

### Threshold Algorithm

The lowest lying isomers produced in the BCGA optimisation step are used as starting points for threshold analysis. The threshold algorithm[31,50] combines a Monte Carlo random walk in configuration space below a predefined maximum energy value (threshold or lid) with systematic quenches to low-lying states. In this way, the energy landscape local to the starting minimum may be mapped fairly exhaustively, whilst searching further afield for new minima is also possible. In the current work, we use Cartesian displacements in one direction for a single atom as the moveclass. The step size is important from the point of view of efficiency. This value is system specific, and is taken to be 0.1 Å for the current work. The lid value is crucial to analysis of barrier structure. Lids confine the walker to pockets of configuration space, or basins, allowing the cluster to move between minima, crossing barriers of energies no higher than the threshold. In this way, small lid values allow us to exhaustively explore well-defined subsets of the landscape, producing locally ergodic regions. Larger values may be

chosen to build up an arbitrarily accurate picture of the barrier structure between minima.

## 2. Results

### 2.1. Gupta Potential Energy Landscape of $Cu_4Ag_4$

The 50:50 composition guarantees the maximal number of possible permutational isomers, $N_H$, which for a binary AB system of $N$ atoms is defined by Equation (5):

$$N_H = \frac{N!}{N_A!(N_B!)} \quad (5)$$

$N_H$ is maximised in the case that $N_A = N_B$, giving a maximum of 70 non-degenerate homotops for each isomer of $Cu_4Ag_4$, and so we may expect a rich energy landscape with two distinct energy scales, one relating to the barriers between structural isomers, the other relating to homotop exchange.

The genetic algorithm is able to find all low-lying isomers, a selection of which are given in Figure 1. The global minimum is found to be the dodecahedral-based structure, with copper atoms occupying the innermost sites. The capped pentagonal bipyramid is almost isoenergetic at +0.056 eV, followed by two forms of bicapped octahedra, at +0.272 and +0.280 eV, denoted BcOh and FCC, respectively. It is notable that the decahedron structure can be converted into a further bicapped octahedron by a small rearrangement in the bond angles and bond lengths of the capping atoms. The next-lowest structure is a tetrahedron-based structure at +0.384 eV, which is tricapped, with the fourth "shell" atom occupying a $\mu$-2 bridging site. This differs slightly from the well-known tetracapped tetrahedron, which is interestingly found to lie much higher in energy at the Gupta level of theory, more than 1 eV above the global minimum. The sixth isomer is a polytetrahedral chain at +0.425 eV, which may be considered as three intertwined chains, forming the basis of a Bernal spiral. This is an exotic motif recently predicted for coinage metal clusters in the sub-nanometre size range.[41] For clusters of twelve atoms and above, the icosahedral motif begins to dominate the low-lying structures, but for octamers, the structures, whilst similarly compact, are predominantly constructed from smaller building blocks—the tetrahedron, octahedron and pentagonal bipyramid. There exist several low-lying homotops of each structure, with energies intermediate between those of the structural motifs, complicating the landscape as expected. For example, there are three homotops of the global minimum at energies lower than that of the first capped pentagonal bipyramid.

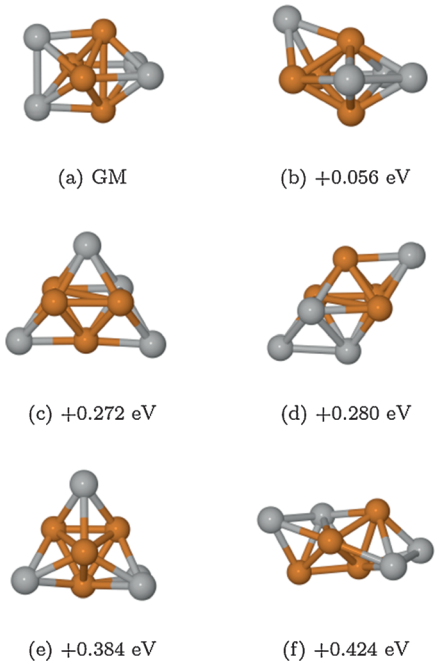


**Figure 1.** The six lowest-energy geometric isomers found from Gupta potential global optimisation, showing compact structures. From (a) to (f), we depict the dodecahedral (dodec), mono-capped pentagonal bipyramidal (McPB), bicapped octahedral (BcOh), another isomer of the bicapped octahedral (FCC), distorted tetracapped tetrahedron (TcTd), and polytetrahedral tetrahelix (helix) geometries.

The preference of homotops that place silver on low coordination sites is strong, and is caused both by the lower surface energy of silver, and also the higher cohesive energy of copper, which is represented in the Gupta potential by the $A$ prefactor of the pairwise repulsive term. This parameter is therefore consistent with the experimental cohesive energies, which are 336 kJ mol$^{-1}$ and 284 kJ mol$^{-1}$ for copper and silver, respectively.

The threshold algorithm is employed with the lowest six isomers as starting structures. For each isomer, the following threshold programme is employed: Eight lids, equally spaced, from −18.56 eV (−2.33 eVatom$^{-1}$) to −18.00 eV (−2.25 eVatom$^{-1}$) are set up, chosen to sample the range from the global minimum to a reasonable energy for stable, sub-optimal structures. For each lid, a simulation is performed in which one walker makes $2.5 \times 10^5$ Monte Carlo steps. Every $10^3$ steps, the walker makes five downhill quenches, which consist of Metropolis MC walks with ($T = 0$), in order to locate low-lying minima. By allowing the walker to make stochastic downhill steps, we allow the same holding point to access multiple minima. In total, we generate 250 stationary points per lid and explore the landscape bounded by an energy up to 0.63 eV above that of the global minimum structure. This is found to be sufficient to interconvert all of the major structural motifs and to find several homotops for each.

Figure 2 shows the trajectory of a typical threshold run. We note that the majority of steps are taken within a small energy range below the maximum value. This is expected, due to the shape of the basins. The number of states within a basin grows approximately exponentially with increasing energy, so higher energy states dominate configuration space. Quenches are shown to converge tightly to minima, of which there are many in a small energy range, which is typical for bimetallic clusters. In some regions of the simulation, we observe that the point in configuration space from which quenches begin is a transition region, finding more than one minimum on local optimisation by quenching.

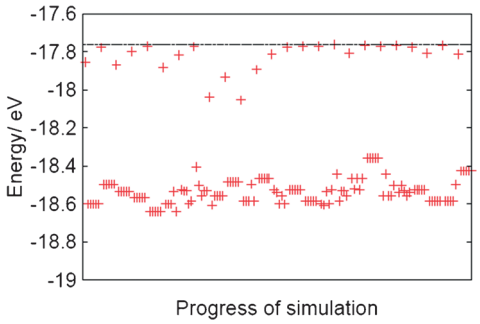


**Figure 2.** Schematic threshold trajectory profile for a simulation with GM at −18.63 eV, and a lid at −17.76 eV. The walker makes moves below the lid (dashed line), and is periodically quenched (lower points).

### 2.1.1. Tree Graph

Tree graphs allow for the visual representation of the energy landscape, by projecting the connectivity of minima along a 1D energy axis. The reduction of dimensionality allows for the direct comparison of the energies of local minima and the lowest-energy transition states that interconvert them, to build a coarse-grained view of the energy landscape as a whole. For the $Cu_4Ag_4$ cluster at the Gupta level of theory, this graph is given in Figure 3, and is produced by considering the results of the threshold run. As the lid energy increases beyond the energetic barrier between a pair of minima, the walker may access the basin region corresponding to the new minimum.

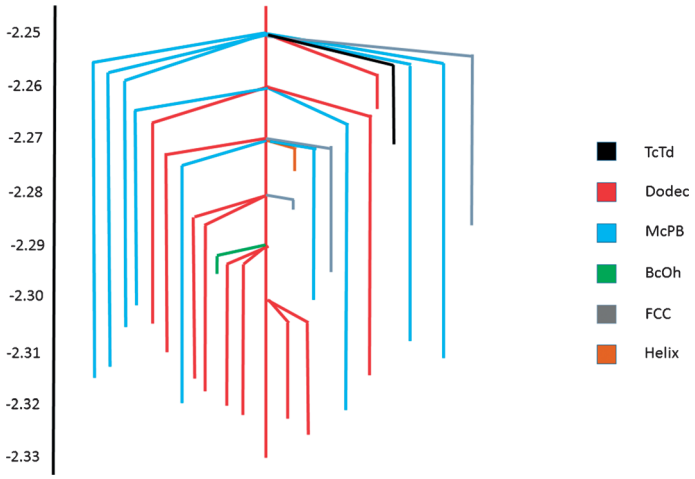


**Figure 3.** Tree graph for the low-lying region of the Gupta $Cu_4Ag_4$ energy landscape. The vertical axis depicts the binding energy per atom in units of $eVatom^{-1}$.

An upper-bound estimate of the transition state energy for the particular interconversion is determined for each pair of minima thus connected. In Figure 3, a tree graph representative of the conversion between each low-lying minimum and the global minimum is shown for a set of lid energies ranging between −2.33 and −2.25 $eVatom^{-1}$ (which corresponds to a total energy range of 0.63 eV). Minima are grouped into structural classes, including the dodec, TcTd, McPB, FCC, BcOh and helix motifs found by global optimisation. It is observed that in the energy range considered, no new structural motifs become available. This implies that while it is not guaranteed that there are no lower-lying minima that have higher barriers to the putative global minimum, they will not be available without a great energy input to perturb the system from the global minimum (or other competitive minima). That other motifs are not found with full global optimisation with the BCGA also supports the conclusion that there are no such additional structures in the low-energy range.

It is notable that the tree graph is dominated by two geometries, the dodec and the McPB clusters, which make up a large proportion of the total minima found, and additionally are the lowest-energy pair of structures. This result suggests that the two motifs make up a significant fraction of configuration space in the low-energy range, and that many of the homotops of the two structures are lower in energy than any homotop of any other geometry. Therefore, the landscape is hierarchical, with a separation of energy scales between the permutational isomers of each structure, and the different structural motifs. It is not generally true however, that the landscape which results is without frustration. In the case of the McPB motifs, the barriers to convert to the GM (dodec) are remarkably high, even for minima which are low in energy. This frustration reduces the probability of interconverting motifs, despite similarity in the final energy of the endpoints, and leads to a dominance of the dodecahedral motif.

The higher-lying structural motifs are severely under-represented in the tree graph, with only one example of the BcOh, TcTd and helix, and two homotops of the FCC geometry in the energy range considered. There are two causes for this under-representation. Firstly, the basins which contain these minima occupy smaller regions of configurational space, and are less frequently sampled by the MC walker during the simulation, which may be explored by analysis of the density of states (DOS). Secondly, the barriers to interconversion between these motifs and the global minimum are high. Both explanations lead to the result that these structures are unlikely to be observed, according to the Gupta potential.

### 2.1.2. Probability Flow

Sampling the distribution of minima found on quenching during threshold runs provides statistical information on the rearrangements of the cluster. If the sampling of the region $R(L)$ available to the walker for a given lid $L$ is ergodic, it may be stated that the occupation probabilities of the available minima are proportional to their equilibrium values within this region, as long as we are considering temperatures low enough to prevent a walker from leaving the region on the observational time scales of interest, $t_{obs} \ll \tau_{esc}(R;T)$. The probability flows measured for a given lid value provide insight into the speed with which the equilibrium inside the pocket $R(L)$ below the energy lid can be established. We note that the maximal tem-

perature $T_{max}(L)$ for which we can achieve equilibrium in the pocket is to a certain extent correlated with the chosen lid value. Similarly, by comparing the probablity flow between minima at various lid values, we can observe how the flow varies with lid energy, and thus draw conclusions regarding the size of the entropic barriers between the minima inside the pocket as function of temperature, as long as $T < T_{max}$, that is, as long as we stay within the pocket defined by the lid $L$. As a consequence, the temperature not only restricts access to new basins, and thus minima, but alters the probabilities of the available transitions beyond the straightforward Arrhenius-type effect.

Figure 4 shows the flow for the lowest-energy homotops of the two more favourable structural motifs, the dodec and the

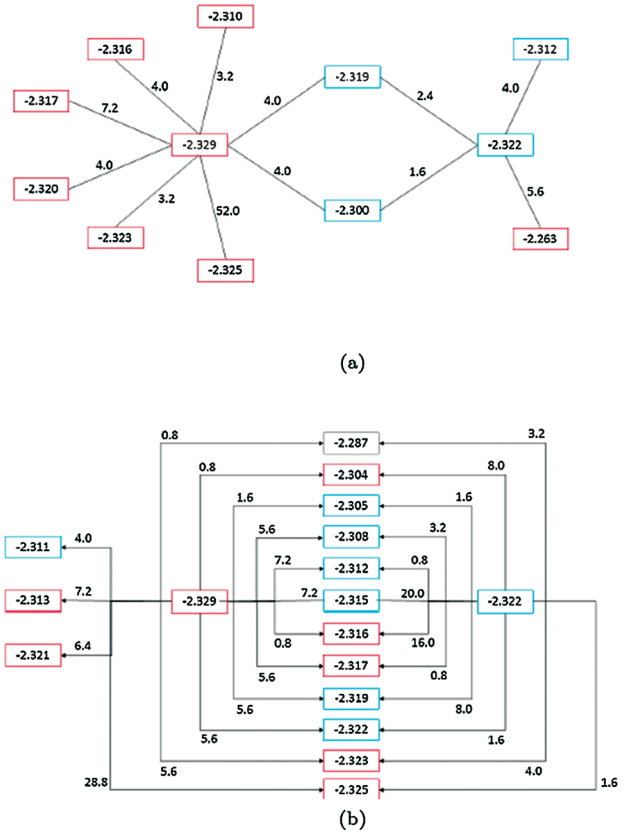


**Figure 4.** Probability flow between the lowest-energy homotops of dodec ($-2.329$ eVatom$^{-1}$) and McPB ($-2.322$ eVatom$^{-1}$), at lids of a) $-2.27$ eVatom$^{-1}$ and b) $-2.25$ eVatom$^{-1}$. The minima are coloured consistently with the key in Figure 3, and the percentages for the transition are shown along the lines which interconnect minima. Return probabilities are for the dodec 18.4% and 8.2%, and for the McPb are 86.4% and 31.2% for the lower and higher lids, respectively.

McPB clusters. The analysis is performed for two lid values, $-2.27$ eVatom$^{-1}$, which is the lowest lid that allows the interconversion of these minima, and a higher energy, $-2.25$ eVatom$^{-1}$, which allows the rearrangement between the GM and all of the isomers found in the study. The percentage of quenches which lead to a particular minimum is given as the number on the line connecting the pair of minima. Minima are labelled by their total energy per atom, and coloured according to the key in Figure 3. The total sum of probability flow percentages equals 100 if the return probability to the starting minimum is taken into account (given in the caption).

From the lower energy lid, it is notable that the dodec minimum predominantly finds other dodec minima, and that there is one dominant minimum, which is found in 52% of quenches. This homotop is the first suboptimal minimum, and is also the structure located with the lowest barrier of all minima. At a lid of $-2.27$ eVatom$^{-1}$ it may be said that the two minima belong to a locally ergodic region. In fact, the run which starts at the GM structure quenches to this minimum more frequently than returning to the starting structure, which is found in 18.4% of quenches. The McPB minimum, at $-2.322$ eVatom$^{-1}$ escapes its basin much less frequently, suggesting barriers to other structures are higher for this minimum than the global minimum. Interestingly, the two minima do not interconvert directly. From either starting point, none of the quenches along the threshold run trajectories reached the other endpoint. This result is at variance with that of the tree graph, which shows it is energetically possible to interconvert this pair at $-2.27$ eVatom$^{-1}$. The dynamic view of the probability flow shows that while there is a transition region below the lid that allows the rearrangement, the pathway is difficult to traverse. This is likely to be due to a narrow path through configurational space with few states, and thus a low statistical weight, and is an example of a configurational entropic barrier, whereby the energy required to interconvert minima, in practice, is higher than the minimum energy defined by the transition region. There are minima which are reached by both starting structures, which in the case of the low-energy lid are both McPB structures. From both endpoints, the flow is very small, and so these intermediate McPB structures do not provide good alternative routes to interconvert the endpoint structures.

For the higher-energy lid, it is possible to reach a large number of additional minima from either endpoint, and so the flow diagram contains many more minima. It may qualitatively be stated that the sampling of the low-lying regions of the landscape are considerably more ergodically sampled for a lid of $-2.25$ eVatom$^{-1}$ than $-2.27$ eVatom$^{-1}$. Further, it is notable that almost all minima which may be reached are found by both starting structures. This means that indirect conversion, whilst low in frequency for most paths, combines to produce many routes between the endpoints, with a high overall statistical weight. Furthermore, there is a route to direct rearrangement, as observed for the pathway with frequency 5.6% from $-2.329$ eVatom$^{-1}$ (dodec GM) to $-2.322$ eVatom$^{-1}$ (lowest McPB). Remarkably, there is no direct reverse route, which implies that there is a large entropic barrier for the backward rearrangement. That this occurs, suggests the dynamics of the McPB basin is dominated by other structures, and few routes lead to the GM. The ergodicity of most paths is evident from the reduced bias of either starting structure to motifs of its own kind, and from the reduction in self-quenching. The GM is trapped in its own basin for only 8.2% of quenches, as compared with 18.4% for the lower lid.

### 2.1.3. Density of States

The density of configurational states is defined by Equation (6):

$$n(E) = \sum_{E} g(E)dE \tag{6}$$

where $dE$ is a small energy interval, or equivalently, the width of the energy bin over which we sample states, $g(E)$ is the local density of states which results from sampling the local landscape with that bin size, and $n(E)$ is the total number of configurational states from summation over the range of $E$ bounded from below by the energy of the local mimimum, and from above by the energy of the lid. By sampling every step during the simulation, we gather density of states profiles for $2.5\times10^5$ steps per lid. The growth of the density of states with lid energy is then calculated by connecting the local DOS gathered for each lid and renormalising.

As the growth rates are calculated for each lid and connected, the profile for the density of states available from a given starting minimum can be produced. The profiles from each individual starting mininum share a common gradient when the basins that contain the minima have merged, providing an additional statistical definition of the interconversion barriers.

In Figure 5, we observe that for the low-lying structural motifs of the Gupta landscape, there is a separation of $g(E)$ between the dodec and McPB structures, and the other, higher-lying motifs. The total basin volume in configurational space, as approximated by the DOS, is considerably larger for McPB than for other structures. It is unremarkable that the basins for FCC and BcOh minima are very similar, both in growth rate with energy and total number of states, as they are quite similar structures, interconverted by single migrations of atoms. However, it is of note that the helical cluster, which is structurally distinct from all other low-energy minima, has a similar DOS growth profile to BcOh and FCC. This cluster has considerably lower symmetry, and is based on face-sharing tetrahedral subunits, rather than the octahedron, and so it is not necessary that the classes should share statistical similarities. The helix,

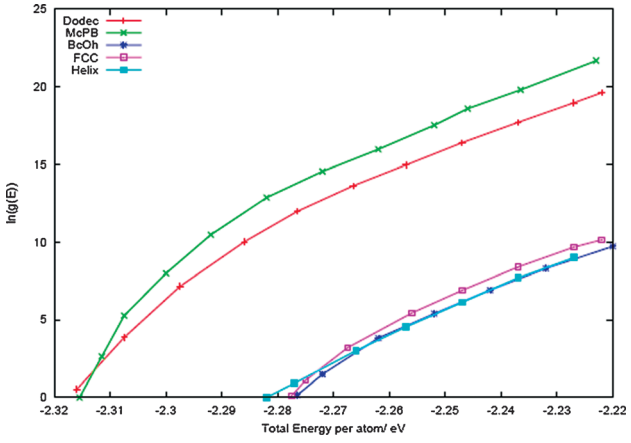


**Figure 5.** DOS profiles of low-lying Gupta minima showing the growth with energy.

FCC and BcOh motifs all join the superbasin of the dodec/McPB at approximately equal energies, below $-2.27$ eVatom$^{-1}$, which is in agreement with the results from the connectivity analysis. This implies not only that the growth of their basins is marginal, as given by the slope of their profiles, but that these minima belong to basins of small total volume. By contrast, the growth rates are much higher for McPB and dodec structures and, owing to their lower energies, have basins that grow to large total volumes before merging with the higher-lying minima. It is interesting that the McPB motif has a higher rate of DOS growth than the dodec, such that the total volume of the basin will be larger, and the total DOS exhibits a crossing at 0.007 eVatom$^{-1}$ (56 meV) above the GM energy. This results in an additional frustration effect whereby the lowest-energy structure is not statistically the most likely to be found through a quench from a random starting geometry and the high barrier to interconversion between McPB and dodec motifs further reinforces this trapping.

The structure of the landscape may be considered to consist of two large basins corresponding to McPB, and several small basins which connect to the large dodec/McPB superbasin at similar energies.

## 2.2. DFT Landscape of $Cu_4Ag_4$

Global optimisation at the DFT level produces a set of low-lying structures with some similarity to those found with the Gupta potential, although the ordering of energies varies between methods, as shown in Figure 6. Most strikingly, the tetracapped tetrahedron is found to be the global minimum at the DFT level, whereas the equivalent member of that class is more than 1 eV higher than the GM at the Gupta level. This geometry is optimal at the DFT level due to the stronger effect of surface energy and size differences between copper and silver from the DFT calculations, whilst charge transfer from copper to silver, an effect which is absent from the semi-empirical potential also plays some role in favouring the capping of copper by silver, as explained in Ref. [8]. The dodec, McPB and BcOh motifs are again found to be fairly low-lying, at binding energies relative to their global minima of $+0.200$ eV ($+0.025$ eVatom$^{-1}$), $+0.400$ eV ($+0.05$ eVatom$^{-1}$) and $+0.432$ eV ($+0.054$ eVatom$^{-1}$) respectively. The preferred homotop is identical between levels of theory for all three of these structures, although the bond lengths are noticeably changed.

There are additional structures which are not present in the Gupta simulation, including a buckled pentagonal-based structure, the lowest-energy variant of which lies at $+0.160$ eV ($+0.02$ eVatom$^{-1}$), and a capped trigonal prismatic structure at $+0.328$ eV ($+0.041$ eVatom$^{-1}$). These forms are more open than the previously found geometries, and represent a class which become dramatically stabilised at DFT level relative to the empirical potential. The Gupta potential is known to overestimate the strength of metal–metal bonding, such that compact structures are too greatly preferred. The result is that structures with more severe undercoordination and pseudo-planar geometries become stabilised by DFT. It is notable that

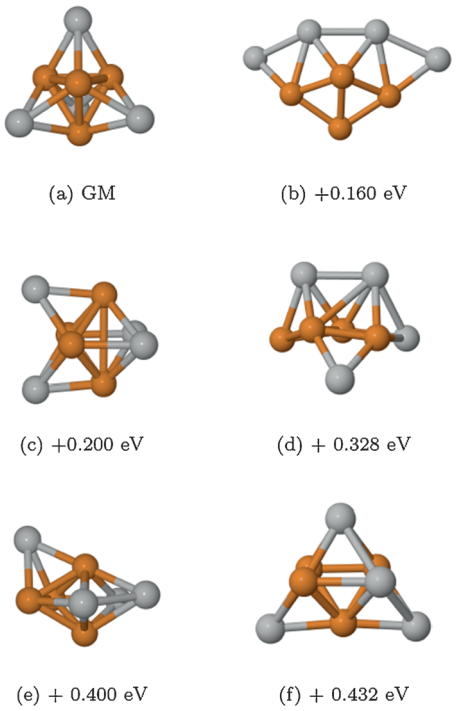


**Figure 6.** The lowest-energy geometric isomers as found from DFT global optimisation, showing compact structures. From (a) to (f), we depict the tetracapped tetrahedron (TcTd), the buckled pseudo-planar bicapped (doubly bridged) pentagon, the dodecahedral-based (dodec) which has now rearranged sufficiently to be better described as an additional bicapped octahedron isomer, the monocapped trigonal prism or capped non-helical polytetrahedron (McTP), the capped pentagonal bipyramid (McPB) and the bicapped octahedron (BcOh) geometries.

even for a system where the global minimum is a compact, three dimensional structure, there are several energetically low-lying open isomers that the empirical potential cannot reproduce. Figure 7 displays the graph of minima which are connected by a single transition state to the TcTd global minimum, with a scale of cohesive energy (in eVatom$^{-1}$), determined with respect to the reference of neutral atoms, which is analogous to the binding energy for the clusters calculated with the Gupta potential. The graph shows a maximum transition state barrier of $-0.24$ eVatom$^{-1}$, which is 2.4 eV (0.3 eVatom$^{-1}$) above the GM. Within this range, there is a more even distribution of minima than found for Gupta, with several homotops found for all six of the structural classes. Furthermore, it is striking that while the differences in total energy between minima are similar for the two levels of theory, the barriers for the DFT rearrangements are significantly higher. Very few minima are interconverted until the barrier height reaches $-0.29$ eVatom$^{-1}$ (GM + 2.08 eV), at which point many new basins become accessible. Higher barriers to rearrangement between similar structural motifs were observed in a previous threshold algorithm study for $MgF_2$ clusters,[40] with DFT (B3LYP functional) and a Coulomb-plus-Buckingham-type potential. The necessity to attain high energies in order to increase the variety of potential minima suggests that frustration is even greater in the case of the DFT energy landscape. It is interesting to note that there are a large number of distinct minima, belonging to several structural classes that are essentially degenerate, between $-0.49$ eVatom$^{-1}$ (GM + 0.4 eV) and $-0.39$ eVatom$^{-1}$ (GM + 0.5 eV), despite the varying barrier heights which allow access to them.

## 3. Discussion

The various statistical analyses applied to the clusters allow for a semi-quantitative view of the energy landscape to emerge, in which the hierarchy of energy scales, the frustration inherent in the topology of the surface and particular information, for each basin, about the growth and shape of the basin are available. From the tree graph, the probability flows and the DOS profiles, this information is combined, and it is observed that the results are complementary. The energies at which the various basins merge with that of the global minimum is consistent from the tree graph and the DOS curves, while the latter additionally provide information on the size of the basins. It is interesting to note that there is not a strong correlation between the growth rate of the basin with energy and the energy of the minimum. While the lowest two minima correspond to the largest basins with highest growth rates, the GM has a lower growth rate than the first suboptimal structure, and the BcOh, FCC and helical clusters, which differ in minimum energy by 0.15 eV (0.019 eVatom$^{-1}$), have essentially equivalent growth rates and densities of states. The total volume of the basins that contain the high-energy minima are however smaller than the lower-energy basins, as to a reasonable approximation, the height of the barrier corresponds to

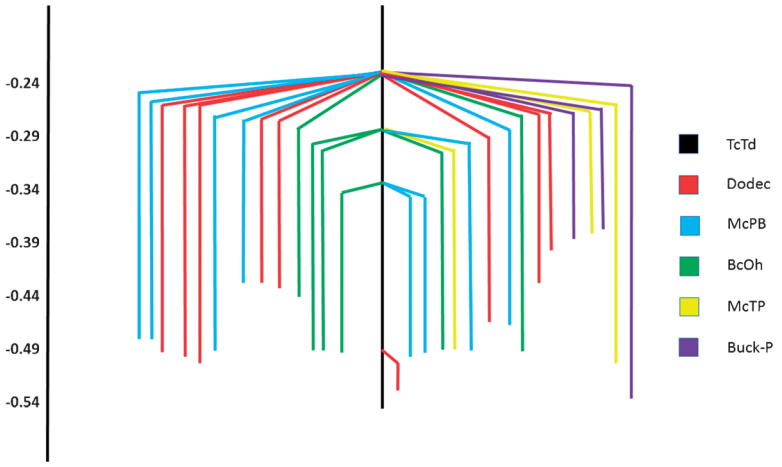


**Figure 7.** Tree graph for minima directly connected to the global minimum at the DFT level. The vertical axis depicts the cohesive energy per atom in units of eVatom$^{-1}$.

the depth of the minimum. While clearly not general, similar observations have been made in studies of energy landscapes that exhibit a certain degree of self-similarity,[51] and, with some exceptions for McPB structures, it is found for the Gupta $Cu_4Ag_4$ cluster. Such a barrier structure implies that, on average, high-lying minima are converted into low-lying ones with relatively low activation energy costs, if the transition begins at the high-lying structure. As a result, the basin which contains the less stable structure does not reach a large volume before connecting with that of the more favourable structure. Still, one should keep in mind that the higher-lying minimum can be stabilised by entropic barriers;[38] such an entropic stabilisation can even result in differing growth laws of the sampled local densities of states at energies above the minimal energy barrier separating the two minima.[37]

Application of the threshold method to clusters at the DFT level allows for comparison with the Gupta potential. The $Cu_4Ag_4$ cluster was selected due to its known preference for compact, pseudo-spherical structures, as noted in DFT studies, and from experimental work on both $Ag_8$ and $Cu_8$, for which both clusters are three-dimensional. By maximising the number of homotops, the study is complicated, and allows for comparison of chemical ordering preference between the two levels of theory. While there is overlap between the structures found to be energetically competitive with the GM for both calculations, it is interesting to note that the Gupta potential gives a different GM, and that the GM at the DFT level is uncompetitive at the Gupta level. The homotop preference is in exact agreement for those structures which are present in both simulations, and so the potential may have utility in predicting chemical order, but there are large classes of structures that do not appear in the Gupta analysis. Polytetrahedral (nonhelical), buckled planar and intersecting planar motifs are found on the DFT landscape, some of which are directly competitive with the global minimum. It is observed that the cost of undercoordination is less severe for the DFT structures than for Gupta clusters, as several motifs exhibit silver atoms in sites which bridge two atoms. Such structures were not found, even after much higher barriers were allowed in Gupta simulations, implying an inability for the potential to stabilise such forms, rather than an incomplete exploration of the landscape. These various, low-symmetry motifs are not often reported in DFT studies of CuAg clusters, and underline the importance of a truly unbiased global exploration of the energy landscape. Furthermore, the need to extend the analysis to high activation barriers is great for the DFT clusters, as the landscape exhibits a large degree of frustration. This frustration is significantly more severe than for the Gupta case, and implies a rougher surface that is more difficult to explore. The result is that while there are many low-lying motifs, several of which are competitive with the GM, and many of which are essentially energetically degenerate with each other, when the cluster finds the TcTd motif, it cannot escape the high transition barriers to find other minima and becomes both energetically and entropically trapped.

## 4. Conclusions

The energy landscape of a prototypical coinage metal bimetallic cluster has been investigated at Gupta and DFT levels of theory. Several statistical tools have been utilised to map the landscape, providing independent and cooperative information which suggests a frustrated system, with distinct energetic hierarchy between homotops and structural motifs at the empirical potential level. The comparison of energetics of minima and transition states between the potential and DFT suggests that while there exists a reasonable degree of overlap between structural classes, the Gupta potential destabilises open, under-coordinated minimum structures which are found to be particularly stable with DFT. The competition between these open minima is close at the DFT level, suggesting that the dominance of 3D structures in previous studies of this cluster is due primarily to the frustration of the landscape, rather than the energetics of the local minima. We propose that global studies of the underlying landscape at the electronic structure level are vital for a complete understanding of even such simple metal cluster systems.

## *Acknowledgements*

*The work has been performed under the HPC-EUROPA2 project (project number: 228398) with the support of the European Commission—Capacities Area—Research Infrastructures. C.J.H. wishes to thank the School of Chemistry, University of Birmingham, and the EPSRC for Ph.D. funding. This research was supported by the University of Birmingham through the BlueBEAR cluster, http://www.bear.bham.ac.uk/bluebear.*

**Keywords:** bimetallics · coinage metals · DFT · energy landscapes · subnanometre clusters

[1] W. de Heer, *Rev. Mod. Phys.* **1993**, *65*, 611 – 676.
[2] M. Brack, *Rev. Mod. Phys.* **1993**, *65*, 677 – 732.
[3] A. Fielicke, I. Rabin, G. Meijer, *J. Phys. Chem. A* **2006**, *110*, 8060 – 8063.
[4] F. Furche, R. Ahlrichs, P. Weis, C. Jacob, S. Gilb, T. Bierweiler, M. M. Kappes, *J. Chem. Phys.* **2002**, *117*, 6982.
[5] H. Häkkinen, M. Moseler, O. Kostko, N. Morgner, M. A. Hoffmann, B. von Issendorff, *Phys. Rev. Lett.* **2004**, *93*, 093401.
[6] V. Bonacic-Koutecký, J. Burda, R. Mitric, G. Zampella, M. Ge, P. Fantucci, *J. Chem. Phys.* **2002**, *117*, 3120.
[7] H. Häkkinen, M. Moseler, U. Landman, *Phys. Rev. Lett.* **2002**, *89*, 033401.
[8] C. J. Heard, R. L. Johnston, *Eur. Phys. J. D* **2013**, *67*, 1 – 6.
[9] L. O. Paz-Borbón, R. L. Johnston, G. Barcaro, A. Fortunelli, *Eur. Phys. J. D* **2009**, *52*, 131 – 134.
[10] G. H. Guvelioglu, P. Ma, X. He, R. C. Forrey, H. Cheng, *Phys. Rev. Lett.* **2005**, *94*, 026103.
[11] R. Fournier, *J. Chem. Phys.* **2001**, *115*, 2165 – 2177.
[12] M. Yang, K. A. Jackson, C. Koehler, T. Frauenheim, J. Jellinek, *J. Chem. Phys.* **2004**, *126*, 024308.
[13] V. Bonacic-Koutecký, V. Veyret, R. Mitric, *J. Chem. Phys.* **2001**, *115*, 10450.
[14] S. Darby, T. V. Mortimer-Jones, R. L. Johnston, C. Roberts, *J. Chem. Phys.* **2002**, *116*, 1536 – 1550.
[15] R. L. Johnston, *Atomic and Molecular Clusters, 1st ed.*, Taylor and Francis, Boca Raton, **2002**.
[16] H. Zhang, T. Watanabe, M. Okumura, M. Haruta, N. Toshima, *Nat. Mater.* **2012**, *11*, 49.

[17] A. Sanchez, S. Abbet, U. Heiz, W. D. Scheider, H. Häkkinen, R. N. Barnett, U. Landman, *J. Phys. Chem. A* **1999**, *103*, 9573 – 9578.
[18] J. C. Idrobo, W. Walkosz, S. F. Yip, S. Ögüt, J. Wang, J. Jellinek, *Phys. Rev. B* **2007**, *76*, 205422.
[19] V. Bonacic-Koutecký, M. Boiron, J. Pittne, P. Fantucci, J. Koutecký, *Eur. Phys. J. D* **1998**, *9*, 183.
[20] F. Y. Chen, R. L. Johnston, *Appl. Phys. Lett.* **2007**, *90*, 153123.
[21] F. Cleri, V. Rosato, *Phys. Rev. B* **1993**, *48*, 22 – 33.
[22] A. P. Sutton, J. Chen, *Philos. Mag. Lett.* **1990**, *61*, 139 – 146.
[23] J. N. Murrell, R. E. Mottram, *Mol. Phys.* **1990**, *69*, 571 – 586.
[24] L. O. Paz-Borbón, R. L. Johnston, *Computional Studies of Transition Metal Nanoalloys, 1st ed.*, Springer, Amsterdam, **2011**.
[25] G. Rossi, R. Ferrando, A. Rappallo, A. Fortunelli, B. C. Curley, L. D. Lloyd, R. L. Johnston, *J. Chem. Phys.* **2005**, *122*, 194309.
[26] A. Rapallo, G. Rossi, R. Ferrando, B. C. Curley, L. D. Lloyd, G. M. Tarbuck, R. L. Johnston, *J. Chem. Phys.* **2005**, *122*, 194308.
[27] D. J. Wales, *Energy Landscapes With Applications To Clusters, Glasses and Biomolecules*, Cambridge University Press, Cambridge, **2003**.
[28] M. Jansen, K. Doll, J. C. Schön, *Acta. Crystallogr.* **2010**, *66*, 518 – 534.
[29] J. P. K. Doye, M. A. Miller, D. J. Wales, *J. Chem. Phys.* **1999**, *111*, 8417 – 8428.
[30] O. M. Becker, M. Karplus, *J. Chem. Phys.* **1997**, *106*, 1495 – 1517.
[31] J. C. Schön, H. Putz, M. Jansen, *J. Phys. Condens. Matter* **1996**, *8*, 143 – 156.
[32] J. P. K. Doye, D. J. Wales, *Z. Phys. D* **1997**, *40*, 194 – 197.
[33] N. Mousseau, G. T. Barkema, *Phys. Rev. E* **1998**, *57*, 2419 – 2424.
[34] G. J. Rylance, R. L. Johnston, Y. Matsunaga, C.-B. Li, A. Baba, T. Komatsuzaki, *Proc. Natl. Acad. Sci. USA* **2006**, *103*, 18551.
[35] L. C. Smeeton, M. T. Oakley, R. L. Johnston, *J. Comput. Chem.* **2014**, *35*, 1481 – 1490.
[36] S. Heiles, R. L. Johnston, *Int. J. Quantum Chem.* **2013**, *113*, 2091 – 2109.
[37] M. A. C. Wevers, J. C. Schön, M. Jansen, *J. Phys. Condens. Matter* **1999**, *11*, 6487 – 6499.
[38] J. C. Schön, M. A. C. Wevers, M. Jansen, *J. Phys. Condens. Matter* **2003**, *15*, 5479 – 5486.
[39] J. C. Schön, Z. P. Cancarevic, A. Hannemann, M. Jansen, *J. Chem. Phys.* **2008**, *128*, 194712.
[40] S. Neelamraju, J. C. Schön, K. Doll, M. Jansen, *Phys. Chem. Chem. Phys.* **2012**, *14*, 1223 – 1234.
[41] R. Pacheco-Contreras, M. Dessens-Félix, D. J. Borbón-Gonzalez, L. O. Paz-Borbón, R. L. Johnston, J. C. Schön, A. Posada-Amarillas, *J. Phys. Chem. A* **2012**, *116*, 5235 – 5239.
[42] S. Nunez, R. L. Johnston, *J. Phys. Chem. C* **2010**, *114*, 13255 – 13266.
[43] F. Baletto, C. Mottet, R. Ferrando, *Phys. Rev. B* **2002**, *66*, 155420.
[44] P. Giannozzi, S. Baroni, N. Bonini, M. Calandra, R. Car, C. Cavazzoni, D. Ceresoli, G. L. Chiarotti, M. Concoccioni, I. Dabo, A. Dal Corso, S. de Gironcoli, S. Fabris, G. Fratesi, R. Gebauer, U. Gerstmann, C. Gougoussis, A. Kokalj, M. Lazzeri, L. Martin-Samos, N. Marzari, F. Mauri, R. Mazzarello, S. Paolini, A. Pasquarello, L. Paulatto, C. Sbraccia, S. Scandolo, G. Sclauzero, A. P. Seitsonen, A. Smogunov, P. Umari, R. M. Wentzcovitch, *J. Phys. Condens. Matter* **2009**, *21*, 395502.
[45] A. M. Rappe, K. M. Rabe, E. Kaxiras, J. D. Joannopoulos, *Phys. Rev. B* **1990**, *41*, 1227 – 1230.
[46] J. P. Perdew, K. Burke, M. Ernzerhof, *Phys. Rev. Lett.* **1996**, *77*, 3865 – 3868.
[47] M. Methfessel, A. T. Paxton, *Phys. Rev. B* **1989**, *40*, 3616 – 3621.
[48] R. L. Johnston, *Dalton Trans.* **2003**, 4193 – 4207.
[49] S. Heiles, A. J. Logsdail, R. Schäfer, R. L. Johnston, *Nanoscale* **2012**, *4*, 1109 – 1115.
[50] J. C. Schön, *Ber. Bunsen-Ges.* **1996**, *100*, 1388 – 1391.
[51] J. C. Schön, P. Sibani, *Europhys. Lett.* **2000**, *49*, 196 – 202.

Received: December 16, 2014
Published online on March 17, 2015